In memory of S. M. Nelson

A Realistic Model for Heme-containing Catalases and Peroxidases: the *X*-Ray Structural Characterisation† of a Non-porphyrin Iron(III) Macrocyclic Complex, and the Mechanism of Its Peroxidation of Aromatic Substrates

Colin J. Cairns
Department of Chemistry, Drake University, Des Moines, Iowa 50311, U.S.A.
Roger A. Heckman
ARCO Chemical Co., 3801 West Chester Pike, Newton Square, Pennsylvania 19078, U.S.A.
Alexandra C. Melnyk
Chemical Abstracts Service, 2540 Olentangy River Road, Columbus, Ohio 43202, U.S.A.
William M. Davis and Daryle H. Busch*
Department of Chemistry, The Ohio State University, Columbus, Ohio 43210, U.S.A.

In acidic buffered aqueous solution the complex dichloro{*meso*-2,12-dimethyl-3,7,11,17-tetraazabicyclo[11.3.1]heptadeca-1(17),13,15-triene}iron(III) tetrafluoroborate, [Fe(*meso*-L')Cl_2]BF_4, exhibits both catalase- and peroxidase-like activity. The predominant cation in aqueous buffered solution at pH 4.65 is the mixed species [Fe(*meso*-L')(OH)(H_2O)]$^{2+}$. The catalase- and peroxidase-like activity is proposed to occur *via* a high oxidation state intermediate rather than through involvement of free hydroxyl radicals. Quantitative compliance with the algebraic forms of theoretical rate laws fails to distinguish between these possibilities. However, the kinetics of dioxygen evolution in the presence of hydroxyl radical traps leads to the elimination of the hydroxyl radical model. In addition, the peroxidase-like reactivity of substituted benzenes toward the [Fe(*meso*-L')(OH)(H_2O)]$^{2+}$–H_2O_2 model system parallels that expected for an electrophilic oxidant, and not that of free OH radicals. Parallel experiments with Fenton's reagent support this view. An *X*-ray structural determination on the dichloro complex indicates that the macrocycle adopts a folded conformation allowing the two chloride ligands to occupy *cis* positions in the co-ordination sphere. This stereochemistry is proposed to be retained in aqueous solution, and may allow bidentate co-ordination of hydrogen peroxide, a structural feature that may be critical to the catalase- and peroxidase-like activity. The iron(III) complex crystallises in the orthorhombic system, a = 10.046(2), b = 13.322(2), c = 15.262(3) Å, space group *Pnma*, with four molecules per unit cell. Final residuals had values of 0.042 and 0.043, for R and R', respectively, upon convergence for 1 525 observed reflections. Both the cationic, macrocyclic complex and the BF_4 anion display crystallographically imposed mirror symmetry. The iron(III) ion displays an approximately octahedral geometry, with co-ordination angles ranging from 77 to 95°. An analysis of associated torsion angles suggests that the folded conformation of the macrocycle is almost strain free.

Of the many processes controlled by the heme proteins, the catalysed decomposition of hydrogen peroxide is the easiest to reproduce in synthetic systems. Many studies have been devoted to this process, and to the closely related one in which the decomposition of peroxide is coupled to peroxidation of suitable substrates. These studies can be subdivided into those in which a metalloporphyrin is the catalyst, and those involving a non-porphyrin complex. Iron(III)[1-3] and manganese(III)[3,4] porphyrins have been most commonly studied in the former category, while the latter group includes iron(III) complexes with ligands ranging from water[5] and acetonitrile[6] to chelating molecules such as acetylacetone,[7] ethylenediaminetetra-acetic acid (H_4edta),[8] catechol (1,2-benzenediol)[9] and triethylene-tetra-amine.[10]

The mechanistic pathways involved in the catalase- and peroxidase-like behaviour of these model systems can likewise be described under two general headings. The mechanism generally accepted for the action of the hydrated ions of iron in the catalytic decomposition of H_2O_2 and attendant oxidation of organic substrates (HR)[11,12] (Scheme 1) involves the free hydroxyl radical as the active oxidant. On the other hand, peroxidase, catalase, and cytochrome P450 probably react *via* high-valent oxoiron (FeO^{3+}) intermediates,[1b,13-17] which have been implicated in their catalytic cycles. In Scheme 2, HP stands for heme protein, which may be catalase or peroxidase; H_2A represents a general inhibitor. Equations (9) and (10) represent catalase-like action while equations (9), (11), and (13) represent peroxidase-like activity. The main feature of this cycle is the occurrence of well documented[17] chemical intermediates with a high oxidation level for the central iron and the porphyrin ligand. Other iron(III) chelates have been proposed to react with peroxide by pathways which bear some similarity to the enzymatic cycle in that they involve a resonance-stabilised oxoiron intermediate. The system of Hamilton *et al.*,[9] involving $Fe^{III}_{(aq)}$–H_2O_2–1,2-benzenediol, is an example. An exception to this categorisation is the [Fe(edta)]$^-$–H_2O_2 system, where a recent study[8] has led to the proposal that the rate-determining step in catalase-like activity is breakdown of an [Fe(edta)]$^-$

† *Supplementary data available:* see Instructions for Authors, *J. Chem. Soc., Dalton Trans.*, 1987, Issue 1, pp. xvii—xx.

$$H_2O_2 + (Fe^{3+}) \xrightarrow{k_1} (Fe^{2+}) + H^+ + HO_2^{\bullet} \quad (1)$$

$$(Fe^{2+}) + H_2O_2 \xrightarrow{k_2} (Fe^{3+}) + HO^- + HO^{\bullet} \quad (2)$$

$$HO^{\bullet} + H_2O_2 \xrightarrow{k_3} H_2O + HO_2^{\bullet} \quad (3)$$

$$HO_2^{\bullet} + (Fe^{3+}) \xrightarrow{k_4} O_2 + (Fe^{2+}) + H^+ \quad (4)$$

$$HO_2^{\bullet} + (Fe^{2+}) \xrightarrow{k_5} HO_2^- + (Fe^{3+}) \quad (5)$$

$$OH^{\bullet} + HR \xrightarrow{k_6} H_2O + R^{\bullet} \quad (6)$$

$$R^{\bullet} + O_2 \xrightarrow{k_7} RO_2^{\bullet} \quad (7)$$

$$RO_2^{\bullet} + (Fe^{2+}) \xrightarrow{k_8} RO_2^- + (Fe^{3+}) \quad (8)$$

Scheme 1.

$$H_2O_2 + HP \underset{k_{-9}}{\overset{k_9}{\rightleftharpoons}} [Fe^{4+}(O^{2-})(P^{\bullet-})] + H_2O \quad (9)$$

$$[Fe^{4+}(O^{2-})(P^{\bullet-})] + H_2O_2 \xrightarrow{k_{10}} [Fe^{3+}(P^{2-})] + O_2 + H_2O \quad (10)$$

$$[Fe^{4+}(O^{2-})(P^{\bullet-})] + H_2A \xrightarrow{k_{11}} [Fe^{4+}(O^{2-})(P^{2-})] + HA^{\bullet} \quad (11)$$

$$[Fe^{4+}(O^{2-})(P^{2-})] + H_2A \xrightarrow{k_{12}} [Fe^{3+}(P^{2-})] + HA^{\bullet} \quad (12)$$

$$2HA^{\bullet} \longrightarrow A + H_2A \quad (13)$$

Scheme 2.

peroxy intermediate (although hydroxyl radicals are involved in decomposition processes as the reaction proceeds).

As part of our program of studies directed toward totally synthetic biomimetics for heme proteins, we have previously reported[18] the detailed solution behaviour of an iron(III) complex of the tetradentate macrocyclic ligand *meso*-L′, $[Fe(meso\text{-}L')(OH)(H_2O)]^{2+}$, which acts as a catalyst for the rapid decomposition of hydrogen peroxide.

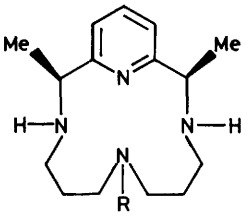

L′; R = H
L″; R = Me

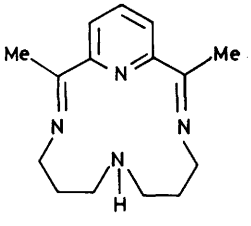

L

The rate law for the initial reaction in the presence of an acetate buffer can be formulated as either equation (14) or (15).

$$\text{Rate} = \frac{k_a[cat][H_2O_2]^2}{[H^+](1 + K_a[O_2CMe^-])} \quad (14)$$

$$\text{Rate} = \frac{k_b[cat][H_2O_2]^2}{[H^+][O_2CMe^-]} \quad (15)$$

(The ambiguity this represents arises from the fact that a plot of the experimental rate of initial dioxygen evolution *vs.* $1/[O_2CMe^-]$ gives a straight line with a near-zero intercept; we are unable to determine whether significance can be attached to this intercept.) This ambiguity is particularly significant since oxidation of the buffer leads to equation (16) in the case of the peroxidase-like mechanism [equivalent to equation (14)], and equation (17) in the case of the radical mechanism [equivalent to equation (15)], where cat represents the catalyst.

$$\frac{d[O_2]}{dt} = \frac{k_9k_{10}[cat][H_2O_2]^2}{k_{-9} + k_{10}[H_2O_2] + k_{11}[HR]} \quad (16)$$

$$\frac{d[O_2]}{dt} = \frac{k_1k_3[cat][H_2O_2]^2}{k_6[HR]} \quad (17)$$

We report here strong indications that a free hydroxyl radical mechanism does not apply, and present a case for a mechanism more allied to the peroxidase-like cycle. Further, we present some data on the peroxidation of aromatic substrates by the $[Fe(meso\text{-}L')(OH)(H_2O)]^{2+}$–$H_2O_2$ system. An *X*-ray structural characterisation of the iron(III) macrocyclic complex used in these studies is also presented. The geometry adopted by the complex in the solid state, and also in solution, may have a bearing on the mechanism of catalase- and peroxidase-like activity.

Experimental

All chemicals were reagent grade and used without further purification.

Syntheses.—The synthesis of $[Ni(L)(ClO_4)_2]$ has been described.[19] Reduction of this complex to $[Ni(meso\text{-}L')(ClO_4)_2]$ was carried out as follows. The complex $[Ni(L)(ClO_4)_2]$ (20 g, 0.039 mol) was dissolved in water (400 cm^3) at 50 °C. Sodium tetrahydroborate (4 g, 0.11 mol) was added in small portions to the stirred solution over 1 h, keeping the temperature below 65 °C. The reaction mixture was stirred at 50 °C for a further 30 min and filtered hot through Celite. The pH of the filtrate was adjusted to *ca.* 2 by the *careful* addition of 70% $HClO_4$. On cooling deep orange crystals of the essentially pure *meso* isomer were formed in 50% yield. Concentration of the solution gives, successively, a mixture of the *meso* and racemic isomers, and finally the relatively pure racemic complex; this product is lighter in colour than the *meso* isomer. This procedure replaces a more cumbersome one involving catalytic hydrogenation at high pressure.[20]

The synthesis of the ligand *meso*-L′, insertion of iron(II) to form $[Fe(meso\text{-}L')Cl_2]$, and oxidation to give $[Fe(meso\text{-}L')Cl_2]BF_4$, have been described in previous publications.[17,20] The bromide analogue was prepared in a similar manner, using the method of Merrell and co-workers.[21]

Physical Measurements.—The techniques used to study the kinetics of peroxide decomposition by the rate of oxygen evolution have been described previously.[18]

The following standard method was developed for oxidation studies on aromatic substrates. To 50 cm^3 of deoxygenated buffer solution (0.02 mol dm^{-3} NaO_2CMe–$MeCO_2H$, pH 4.65, made up to 0.1 mol dm^{-3} ionic strength with KNO_3) under an inert atmosphere was added $[Fe(meso\text{-}L')Cl_2]BF_4$ (0.05 g, 0.1 mmol). When the catalyst had dissolved the organic substrate (2.2—6.4 mmol) was added and the mixture was stirred vigorously to achieve dispersion of immiscible substrates in the aqueous layer. Hydrogen peroxide {50 cm^3, *ca.* 1 mol dm^{-3}; standardised by titration of a 3% solution against 0.1 mol dm^{-3} $[NH_4]_2[Ce^{IV}(NO_3)_6]$ stabilised with 1 mol dm^{-3} H_2SO_4, using ferroin [tris(1,10-phenanthroline)iron(2+)] as indicator} was added in bulk. Dioxygen evolution was usually complete after a few seconds; at this point the reaction was quenched by addition of 2 mol dm^{-3} H_2SO_4 (40 cm^3). The reaction mixture

Table 1. Final fractional co-ordinates for [Fe(*meso*-L′)Cl_2]BF_4, with estimated standard deviations (e.s.d.s) in parentheses

Atom	*x*	*y*	*z*
Fe	0.010 33(5)	0.250 00	0.181 55(5)
Cl(1)	0.164 54(11)	0.250 00	0.253 22(11)
Cl(2)	0.075 33(11)	0.250 00	0.046 30(9)
F(1)	0.199 16(35)	0.250 00	0.620 07(36)
F(2)	0.235 03(44)	0.250 00	0.760 38(30)
F(3)	0.326 32(32)	0.139 57(47)	0.666 73(26)
N(1)	−0.061 79(29)	0.250 00	0.304 63(25)
N(2)	−0.004 42(23)	0.041 21(31)	0.209 87(19)
N(3)	−0.139 68(31)	0.250 00	0.122 70(26)
C(1)	−0.087 26(26)	0.134 26(38)	0.341 56(23)
C(2)	−0.141 85(29)	0.130 70(47)	0.417 60(25)
C(3)	−0.169 40(48)	0.250 00	0.454 95(40)
C(4)	−0.046 36(32)	0.010 58(40)	0.298 79(27)
C(5)	−0.051 98(30)	−0.042 00(42)	0.139 87(28)
C(6)	−0.158 03(30)	0.002 35(42)	0.119 94(29)
C(7)	−0.166 04(30)	0.130 50(41)	0.069 80(25)
C(8)	0.035 25(41)	−0.051 83(53)	0.356 88(32)
B	0.274 73(57)	0.250 00	0.680 56(58)

Table 2. Interatomic distances (Å) and angles (°) within the co-ordination sphere of [Fe(*meso*-L′)Cl_2]BF_4, with e.s.d.s in parentheses

Fe–N(1)	2.110(4)	Fe–N(2)	2.151(3)
Fe–N(3)	2.191(4)	Fe–Cl(2)	2.238(2)
		Fe–Cl(1)	2.327(2)
N(1)–Fe–N(2)	77.26(8)	N(1)–Fe–N(3)	87.1(2)
N(1)–Fe–Cl(2)	175.7(1)	N(1)–Fe–Cl(1)	89.1(1)
N(2)–Fe–N(2ⁱ)	154.5(2)	N(2)–Fe–N(3)	89.95(9)
N(2)–Fe–Cl(2)	102.75(8)	N(2)–Fe–Cl(1)	89.21(8)
N(3)–Fe–Cl(2)	88.6(1)	N(3)–Fe–Cl(1)	176.2(2)
		Cl(2)–Fe–Cl(1)	95.27(6)

* Atom indicated by i is at position $x, \frac{1}{2} - y, z$.

was extracted continuously for 4 h with diethyl ether. The diethyl ether solution was reduced to 10 cm^3 and taken up in methanol (50 cm^3), and this solution was analysed for oxidised products. Oxidations using Fenton's Reagent were carried out in an analogous manner using $Fe(SO_4)\cdot 7H_2O$ (1.0 g, 3.6 mmol), H_2O_2 (10.0 cm^3), and *ca.* 5 mmol of aromatic substrate.

A DuPont model 841 high-performance liquid chromatograph was used for the analysis of oxidised products. A Waters μ-C_{18} (reverse phase) and a DuPont Zorbax-SIL (normal phase) column were used. The reverse-phase column was found to be more efficient in separation of the hydroxyacetanilides, using a 30% aqueous methanol mobile phase, and in separating non-polar compounds (such as toluene and bibenzyl) in 75% aqueous methanol. The reactions were quantified using standard curves for the authentic compounds.

X-*Ray Data Collection.*—*Crystal data.* $C_{15}H_{26}BCl_2F_4FeN_4$, M = 475.96 orthorhombic, a = 10.046(2), b = 13.322(2), c = 15.262(3) Å, U = 2 043 Å^3 (by the least-squares refinement of diffractometer angles for 25 reflections with $25 < 2\theta < 30°$, λ = 0.710 69 Å), space group *Pnma*, no. 62 (or *Pna*2_1, no. 33), Z = 4, D_c = 1.54 g cm^{-3}. Light yellow air-stable plates. Crystal dimensions (distances from centre to faces) 0.071(010,0$\bar{1}$0), 0.080(0$\bar{1}$1,01$\bar{1}$), 0.080(011,0$\bar{1}\bar{1}$), 0.095(001,00$\bar{1}$), 0.195(101,$\bar{1}$0$\bar{1}$), 0.0198 mm (10$\bar{1}$,$\bar{1}$01), μ(Mo-K_α) = 10.42 cm^{-1}.

Data collection and processing. Syntex P$\bar{1}$ diffractometer, θ/2θ mode, with scan angles ranging from $K_{\alpha 1}$ −1.0° to $K_{\alpha 2}$ + 1.0° and scan speeds varying from 2.0 to 12.0° min^{-1} in 2θ, Mo-K_α radiation; 2 697 reflections measured ($4 < 2\theta < 55°$; $+h$, $+k$, $+l$), of which 2 251 were unique, $R_{av.}$ = 0.007, ultimately giving 1 525 reflections with $F_o > 6\sigma(F_o)$. No crystal decay was detected in the monitoring of check reflections throughout data collection.

Table 3. Selected torsion angles (°)* for [Fe(*meso*-L′)Cl_2]BF_4

I	J	K	L	Angle
N(1)	C(1)	C(4)	C(8)	170.9
C(2)	C(1)	C(4)	C(8)	−67.1
C(1)	C(4)	N(2)	C(5)	123.9
C(8)	C(4)	N(2)	C(5)	−114.1
C(4)	N(2)	C(5)	C(6)	73.4
N(2)	C(5)	C(6)	C(7)	73.2
C(5)	C(6)	C(7)	N(3)	−71.8
C(6)	C(7)	N(3)	C(7′)	171.3

* Torsion angles IJKL are defined as the angle formed between IJ and KL when viewed along the JK direction. Positive values denote clockwise rotation of IJ into KL and *vice versa.*

Solution and refinement of the structure. The position of the Fe atom was determined by conventional heavy-atom techniques. The choice of space group, either *Pnma* or *Pna*2_1, was ultimately determined by the successful solution of the structure. The remaining non-hydrogen atoms were located by subsequent difference Fourier calculations and least-squares refinement using SHELX 76.[22] All computations were performed on an IBM 3081-D computer. The locations of the amine bound hydrogen atoms were ascertained from difference maps. These were fixed (d_{N-H} = 0.87 Å, U_{iso} = 0.05 Å^2) to their respective atoms in subsequent least-squares refinement. Carbon bound hydrogen atoms were placed in calculated positions (d_{C-H} = 0.95 Å, U_{iso} = 0.07 Å^2 for methylene and aromatic hydrogens and U_{iso} = 0.10 Å^2 for methyl hydrogens). Full-matrix least-squares refinement was carried out with all non-hydrogen atoms varying as anisotropic scatterers. The analysis of the weighting scheme, $w = 1/[\sigma^2(F_o)]$, met the standard criteria for acceptance. Residual electron density in the final difference Fourier map amounted to no more than 0.43 e Å^{-3}. Neutral atom scattering factors for all non-hydrogen atoms were taken from ref. 23, whereas those for hydrogen atoms were taken from the usual source.[24] The final fractional co-ordinates of the non-hydrogen atoms are listed in Table 1. Relevant geometric details are given in Tables 2 (interatomic distances and angles) and 3 (selected torsion angles).

Results and Discussion

The data in Table 4 show the results of rate measurements carried out in the presence of various substances known to compete strongly with H_2O_2 for reaction with the hydroxyl radical. The third column compares the rate constants for the hydroxyl radical reactions of the various inhibitors (HR) [equation (6)] with the rate of reaction of H_2O_2 with the same radical. The values of the rate constants were taken from pulse radiolytic data.[12,25] As the concentration of added inhibitor is much larger than that of hydrogen peroxide, and the inhibitors are much more reactive toward free hydroxyl radicals than is H_2O_2, the rates of oxygen evolution should be decreased greatly in all cases. The complete failure of the hydroxyl radical model to account for the behaviour of this system is emphasised by an application of equation (17), which is derived using that model (Scheme 1). With [buffer] = 0.02 mol dm^{-3}, k_1 is calculated to be 87.6 dm^3 mol^{-1} s^{-1}. This value, and those in columns 2 and 3 of Table 1, yield the values of column 4, the predicted rates of the inhibited reactions. The experimentally observed rates are given in the fifth column of the same table. Within experimental error the observed rates are independent of the concentration of added inhibitor, and differ from those predicted from the radical

Table 4. Effect of HO• substrates on initial oxygen evolution rates ($dm^6\ mol^{-2}\ s^{-1}$) catalysed by $[Fe(meso\text{-}L')(OH)(H_2O)]^{2+}$, [buffer] = 0.02 mol dm^{-3}, I = 0.10 mol dm^{-3}, pH 4.65, T = 25 °C

HR[a]	[HR]	$\left(\frac{k_6[HR]}{k_3[H_2O_2]}\right)^b$	$\frac{\left(\frac{d[O_2]}{dt}\right)}{[cat][H_2O_2]^2} = \frac{k_1k_3}{k_6[HR]}$ Calc.	Observed
HO_2CMe Buffer	0.020	1.2×10^1	7 300	$(7.3 \pm 0.9) \times 10^3$
MeOH	1.7	4.4×10^4	1.9	$(8.5 \pm 1.2) \times 10^3$
EtOH	1.1	5.2×10^4	1.7	$(8.9 \pm 0.5) \times 10^3$
Me_2CO	0.91	1.9×10^3	45	$(7.3 \pm 1.4) \times 10^3$
Me_2CO	1.8	3.8×10^3	22	$(7.7 \pm 1.1) \times 10^3$
Me_2CO	2.7	5.8×10^3	15	$(7.1 \pm 1.3) \times 10^3$

[a] All solutions contain 0.020 mol dm^{-3} buffer. [b] Rate constants[12,25] defined in equations (3) and (6), $[H_2O_2] = 10^{-3}$ mol dm^{-3}.

Table 5. Effect of acetanilide (ad) on the rate of catalytic H_2O_2 decomposition ($dm^6\ mol^{-2}\ s^{-1}$) by $[Fe(meso\text{-}L')(OH)(H_2O)]^{2+}$, $[cat] = 1.0 \times 10^{-3}$ mol dm^{-3}, $[H_2O_2] = 6.4 \times 10^{-2}$ mol dm^{-3}, I = 0.10 mol dm^{-3}, pH 4.65, [buffer] = 0.02 mol dm^{-3}, T = 25 °C

10^2[ad]/mol dm^{-3}	$10^4\left\{\frac{d[O_2]}{dt}\Big/[cat][H_2O_2]^2\right\}$ Calc.	Observed
0	1.30	1.40
0.20	1.20	1.10
0.60	1.00	1.00
1.49	0.79	0.79
1.83	0.72	0.70

model by two to three orders of magnitude. It is therefore concluded that a free radical mechanism is not involved in the catalase-like behaviour of this model system.

Additional results support a peroxidase-like mechanism such as that outlined in Scheme 2. The data in Table 5 show that the initial rate of oxygen evolution decreases in proportion to the amount of acetanilide (ad) added. The results fit a rate law of the form of equation (14) with $k_a = 1.3 \times 10^4\ dm^6\ mol^{-2}\ s^{-1}$ and $K_a = 43\ dm^3\ mol^{-1}$. The earlier study by Melnyk *et al.*[18] contains a large amount of data showing a similar dependence on the buffer concentration. All of these data fit equation (18), where ad represents acetanilide.

$$\frac{d[O_2]}{dt} = \frac{1.5[cat][H_2O_2]^2}{[H^+](1 + 240[HO_2CMe] + 250[ad])} \quad (18)$$

It is reasonable to attribute the specific peroxidatic mechanism of Scheme 3 to the peroxide reactions catalysed by $[Fe(meso\text{-}L')(OH)(H_2O)]^{2+}$. If the hydrogen ion dependence of the rate is ignored this gives a rate law of the form given by equation (23). The mechanism requires that the term $K_{10}[H_2O_2]$ be small compared to the other terms in the

$$[Fe(meso\text{-}L')(OH)(H_2O)]^{2+} + H_2O_2 \underset{k_{-9}}{\overset{k_9}{\rightleftharpoons}} I + H_2O \quad (19)$$

$$I + H_2O_2 \xrightarrow{k_{10}} [Fe(meso\text{-}L')(OH)(H_2O)]^{2+} + O_2 + H_2O \quad (20)$$

$$I + HO_2CMe \xrightarrow{k_{11}} [Fe(meso\text{-}L')(OH)(H_2O)]^{2+} + \text{organic products} \quad (21)$$

$$I + ad \xrightarrow{k'_{11}} [Fe(meso\text{-}L')(OH)(H_2O)]^{2+} + \text{organic products} \quad (22)$$

Scheme 3.

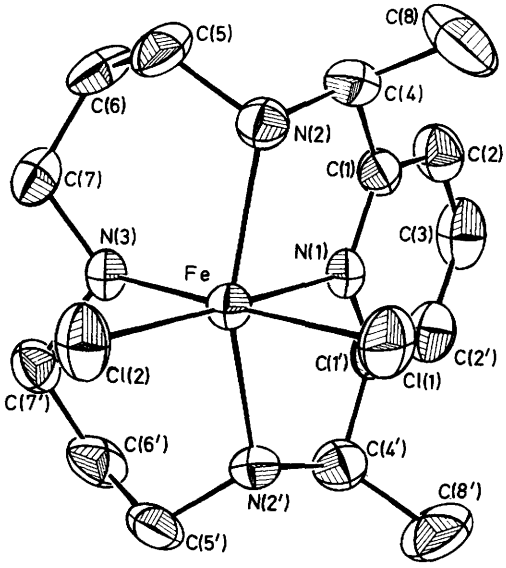

Figure 1. ORTEP view of the macrocyclic cation, $[Fe(meso\text{-}L')Cl_2]^+$. Thermal ellipsoids are depicted at the 40% probability level. The atomic labelling scheme is that used throughout the text. Hydrogen atoms have been omitted for clarity

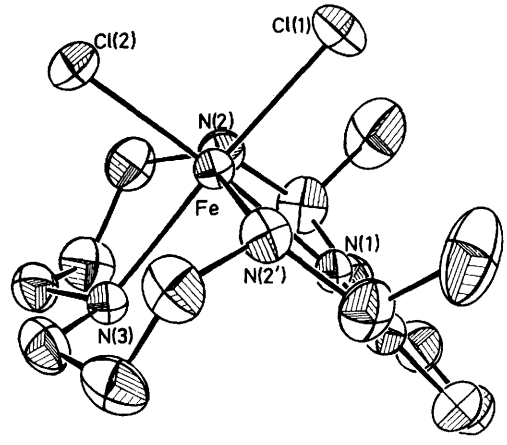

Figure 2. Alternative view of the macrocyclic cation, $[Fe(meso\text{-}L')Cl_2]^+$. Details are the same as in Figure 1

denominator. In addition, one must assume that the active oxidant (I) selectively oxidises acetanilide and the acetate buffer but does not react with acetone or the lower alcohols.

$$\frac{d[O_2]}{dt} = \frac{k_9k_{10}[Fe(meso\text{-}L')(OH)(H_2O)^{2+}][H_2O_2]^2}{k_{-9} + k_{10}[H_2O_2] + k_{11}[HO_2CMe] + k'_{11}[ad]} \quad (23)$$

The peroxidation of acetanilide has been established by h.p.l.c. analysis of the oxidised products. The major products are the 2- and 4-hydroxyacetanilides, with traces only of the 3-hydroxy isomer. The oxidation is clean, with the only other major product being 2,6-diacetylpyridine, formed by decomposition of the catalyst. Table 6 indicates the efficiency and selectivity of this oxidation system when applied to other aromatic substrates. The selectivity is clear from these data; the more electron-rich substrates compete more effectively with H_2O_2 for the active oxidant. Nitrobenzene hardly reacts under the experimental conditions used.

Parallel experiments using Fenton's Reagent,[12] known to be a source of free hydroxyl radicals, produced very little oxidation

Table 6. Selective aromatic oxidation by the system $[Fe(meso\text{-}L')(OH)(H_2O)]^{2+}$–$H_2O_2$, [buffer] = 0.02 mol dm^{-3}, pH 4.65, [cat] = 2.0×10^{-3} mol dm^{-3}, T = 25 °C, volume = 55 cm^3

Moles of reagent			Oxidation products				
Substrate	[Substrate]/mol dm^{-3}	[H_2O_2]/mol dm^{-3}	Moles of product	R	Oxidising equivalent	% Used	% Conversion
Toluene	4.4×10^{-3}	5×10^{-3}	1.0×10^{-3}	9.1	2.4×10^{-3}	24	20
Benzene	6.4×10^{-3}	1×10^{-2}	4.5×10^{-4}	4.0	1.2×10^{-3}	6.0	7
Chlorobenzene	4.5×10^{-3}	1×10^{-2}	3.0×10^{-4}	2.7	6.0×10^{-4}	3.0	7
Acetanilide	2.2×10^{-3}	5×10^{-3}	1.1×10^{-4}	1.0	2.1×10^{-4}	2.1	5
Nitrobenzene	4.1×10^{-3}	1×10^{-2}	1.1×10^{-5}	0.1	2.2×10^{-5}	0.1	0.3

compared with the model system. Only in the case of nitrobenzene were the turnover numbers, defined as the number of moles of oxidation products formed per mole of catalyst (R in Table 6), comparable, and then the value was only 0.1. The amount of hydrogen peroxide used in the reaction, measured by titration of the final reaction mixture against Ce^{IV}, is consistent with the conversion. It should be noted that the reaction system is far from being optimised; the reactions are dilute and heterogeneous and the catalyst lifetime is limited. Nevertheless, at least with the more reactive substrates, appreciable conversion to hydroxylated products occurs.

While the preceding results implicate an electrophilic oxidant as the reactive species they give little clue as to a possible structure for the intermediate. With this in mind, an X-ray analysis was carried out on the catalyst, to identify any structural features which might be important in the catalytic activity. Figures 1 and 2 show two ORTEP[26] views of the macrocyclic cation, and the numbering system used.

The molecule $[Fe(meso\text{-}L')Cl_2]BF_4$ crystallises as discrete ionic units composed of $[Fe(meso\text{-}L')Cl_2]^+$ cations and BF_4^- anions. Both of these species possess mirror symmetry as imposed by crystallographic constraints. The atoms Fe, Cl(1), Cl(2), N(1), N(3), and C(3) of the cation lie upon the mirror plane, as do the boron atom and fluorine atoms F(1) and F(2) of the anion.

The view offered in Figure 2 emphasises the main structural feature exhibited by the cation; the fold which results in the secondary nitrogen N(2) adopting a co-ordination site almost apical to the equatorial plane defined by Fe, Cl(1), Cl(2), N(1), and N(3), *i.e.* the crystallographic mirror plane. The angles N(2)–Fe–A range from 77.26(8) [A = N(1)] to 102.75(8)° [A = Cl(2)] with an average value of 89.8°. The value of the '*trans*' N(2)–Fe–N(2^i) angle reflects considerable distortion from ideal octahedral geometry. The remaining co-ordinated chlorides occupy mutually *cis* positions [Cl(1)–Fe–Cl(2) 95.27(6)°]. As expected, the Fe–N(1) bond distance is shortest, at 2.110 Å. The remaining bond distances and angles are within the range expected for macrocyclic complexes of this type.

The strain involved in folding the macrocycle can be described by the torsion angles, which are listed in Table 3. The only indication of significant strain in this complex is in the torsion angle about the C(4)–N(2) bond. The values of these angles indicate an eclipsed conformation. For the nickel(II) diperchlorate complex[27] the value of the analogous feature is 164°, considerably closer to the completely *anti* configuration. The torsion angles about the sp^2–sp^3 pair C(1)–C(4) have values that indicate[28] further strain in the macrocycle in the vicinity of the aromatic ring. Considerably less strain is evident as one goes around the remainder of the macrocycle. Torsion angle values lying close to the relatively stable *gauche* conformation are noted for all except the C(6)–C(7)–N(3)–C(7^i) unit, which adopts the *anti* configuration. As a consequence of these torsion angles the two six-membered chelate rings adopt flattened chair conformations.

As has just been indicated, a number of X-ray structural analyses have been carried out on complexes of this macrocyclic ligand, and of the very similar one L″ where N(3) is a tertiary nitrogen.[27,29–31] Several studies have shown that folding about the N(2)–M–N(2^i) axis is not uncommon. In addition, spectroscopic evidence shows that copper(II), nickel(II),[20] iron(II),[21] and cobalt(III)[32] complexes of L′ can adopt such a folded conformation if encouraged to do so by the addition of a bidentate chelating ligand, such as oxalate, to complete six-co-ordination around the central ion. Drew and Hollis[29] have structurally characterised an example of such a nickel(II) complex, in which an ethylenediamine completes the co-ordination sphere. Drew *et al.*[32] have also carried out force-field calculations on this complex and on two planar analogues, along with the free ligand. The results indicate that the ligand is quite flexible, in that it can adopt a number of conformations without much difficulty in order to accommodate the central metal ion.

Spectroscopic measurements indicate that the folded conformation exhibited by *meso*-L′ in the solid state is maintained in aqueous solution.[34] Thus, a broad signal at g = 4.2 in the e.s.r. spectrum of the complex in a 2:1 ethylene glycol:buffer (acetic acid–acetate) mixture at −196 °C indicates a rhombic species. It is not unreasonable to propose that an initial step in the catalase- and peroxidase-like activity exhibited by this complex involves co-ordination of H_2O_2 in a bidentate mode, perhaps as the conjugate base HO_2^-. [The pK of 11.25 for this process may be lowered considerably upon co-ordination to iron(III).] This suggestion was made by Wang[10b] in his work on the iron(III)–triethylenetetra-amine–H_2O_2 system, and although that particular system was later found to be rather more heterogeneous than at first thought,[35] the model proposed remains a possibility for these reactive systems. This type of bidentate peroxide co-ordination has been identified by Valentine and co-workers[36] in an iron porphyrin complex. Sugimoto and Sawyer[37] have proposed a 'side-on' bound peroxide intermediate in the peroxidotic action of iron(II) in MeCN solutions. It is suggested that homolytic O–O bond scission, producing an FeO moiety, may be favoured by the strain inherent in the triangular co-ordination of HO_2^- to Fe^{3+}

Conclusions

The $[Fe(meso\text{-}L')(OH)(H_2O)]^{2+}$ catalyst constitutes a realistic model for the enzymatic catalase- and peroxidase-like processes. The selectivity of its reactions is due to the formation of a complex ion intermediate rather than the previously assumed free hydroxyl radical. The structural and electronic properties of the intermediate and a more complete study of the oxidation processes are matters of ongoing research.

Acknowledgements

We thank the National Institutes of Health for support of this work.

References

1 (*a*) S. B. Brown, T. C. Dean, and P. Jones, *Biochem. J.*, 1970, **117**, 741; (*b*) P. Jones, D. Mantle, D. M. Davies, and H. C. Kelly, *Biochemistry*, 1977, **16**, 3974; (*c*) P. Jones, D. Mantle, and I. Wilson, *J. Chem. Soc., Dalton Trans.*, 1983, 161.
2 T. Shimidzu, T. Iyoda, and N. Kanda, *J. Chem. Soc., Chem. Commun.*, 1981, 1206.
3 D. Mansuy, P. Battioni, and J. P. Renaud, *J. Chem. Soc., Chem. Commun.*, 1985, 1255.
4 J. P. Renaud, P. Battioni, J. F. Bartoli, and D. Mansuy, *J. Chem. Soc., Chem. Commun.*, 1985, 888; P. Battioni, J. P. Renaud, J. F. Bartoli, and D. Mansuy, *J. Chem. Soc., Chem. Commun.*, 1986, 341.
5 J. R. Lindsay Smith and R. O. C. Norman, *J. Chem. Soc.*, 1963, 2897.
6 E. Kotani, S. Kobayashi, Y. Ishii, and S. Tobinaga, *Chem. Pharm. Bull.*, 1985, **33**, 4671.
7 M. Tohma, T. Tomita, and M. Kimura, *Tetrahedron Lett.*, 1973, 4359; T. Yamamoto and M. Kimura, *J. Chem. Soc., Chem. Commun.*, 1977, 948.
8 K. C. Francis, D. Cummins, and J. Oakes, *J. Chem. Soc., Dalton Trans.*, 1985, 493.
9 G. A. Hamilton, J. W. Hanafin, jun., and J. P. Friedman, *J. Am. Chem. Soc.*, 1966, **88**, 5269.
10 (*a*) J. H. Wang, *J. Am. Chem. Soc.*, 1955, **77**, 882; (*b*) p. 4715; (*c*) R. C. Jarnagin and J. H. Wang, *ibid.*, 1958, **80**, 786; (*d*) p. 6477.
11 W. C. Bard, J. H. Baxendale, P. George, and K. R. Hargrave, *Trans. Faraday Soc.*, 1951, **47**, 591.
12 C. Walling, *Acc. Chem. Res.*, 1975, **8**, 125.
13 B. Chance, D. S. Greenstein, and F. J. W. Roughton, *Arch. Biochem. Biophys.*, 1952, **37**, 301.
14 M. L. Kremer and G. Stein, *Trans. Faraday Soc.*, 1959, **55**, 959; M. L. Kremer, *Isr. J. Chem.*, 1971, **9**, 321.
15 G. R. Schonbaum and B. Chance, in 'The Enzymes,' ed. P. D. Boyer, Academic Press, New York, 1976, vol. 13, pp. 363—408.
16 J. E. Frew and P. Jones, *Adv. Inorg. Bioinorg. Mech.*, 1984, **3**, 176.
17 J. T. Groves, in 'Cytochrome P-450: Structure, Mechanism and Biochemistry,' ed. P. Ortiz de Montellano, Plenum Press, New York, 1985, ch. 1.
18 A. C. Melnyk, N. K. Kildahl, A. R. Rendina, and D. H. Busch, *J. Am. Chem. Soc.*, 1979, **101**, 3232.
19 J. D. Curry and D. H. Busch, *J. Am. Chem. Soc.*, 1964, **86**, 592.
20 J. L. Karn and D. H. Busch, *Inorg. Chem.*, 1969, **8**, 1149.
21 D. P. Riley, P. H. Merrell, J. A. Stone, and D. H. Busch, *Inorg. Chem.*, 1975, **14**, 490.
22 G. M. Sheldrick, SHELXL User Manual, Nicolet Instrument Co., Madison, Wisconsin, 1981.
23 'International Tables for *X*-Ray Crystallography,' Kynoch Press, Birmingham, 1974, vol. 4, pp. 99, 141.
24 R. F. Stewart, E. R. Davidson, and W. T. Simpson, *J. Chem. Phys.*, 1965, **42**, 3175.
25 L. M. Dorfman and G. E. Adams, National Bureau of Standards Report NSRDS-NBS-46, U.S. Government Printing Office, Washington, D.C., 1973.
26 C. K. Johnson, ORTEP, Report ORNL-3794, Oak Ridge National Laboratory, Tennessee, 1965.
27 M. G. B. Drew and S. Hollis, *Acta Crystallogr., Sect. B*, 1980, **36**, 718.
28 M. F. Bailey and I. E. Maxwell, *J. Chem. Soc., Dalton Trans.*, 1972, 938.
29 M. G. B. Drew and S. Hollis, *Acta Crystallogr., Sect. B*, 1980, **36**, 2629.
30 A. J. Blake, T. I. Hyde, R. S. E. Smith, and M. Schroder, *J. Chem. Soc., Chem. Commun.*, 1986, 334.
31 K. A. Foster, E. K. Barefield, and D. G. Van Derveer, *J. Chem. Soc., Chem. Commun.*, 1986, 680.
32 M. G. B. Drew, D. A. Rice, S. bin Silong, and P. C. Yates, *J. Chem. Soc., Dalton Trans.*, 1986, 1081.
33 E. Ochiai and D. H. Busch, *Inorg. Chem.*, 1969, **8**, 1474.
34 C. J. Cairns and D. H. Busch, unpublished work.
35 M. T. Beck and S. Gorog, *Acta Chim. Acad. Hung.*, 1959, **20**, 57; M. T. Beck and S. Gorog, *Acta Phys. Chem.*, 1958, 70.
36 E. McCandlish, A. R. Miksztal, M. Nappa, A. Q. Sprenger, J. S. Valentine, J. D. Stong, and T. G. Spiro, *J. Am. Chem. Soc.*, 1980, **102**, 4268.
37 N. Sugimoto and D. T. Sawyer, *J. Am. Chem. Soc.*, 1985, **107**, 5712.

Received 26*th November* 1986; *Paper* 6/2287